AIMS Materials Science, 11(6): 1149–1164.
DOI: 10.3934/matersci.2024056
Received: 30 September 2024
Revised: 05 December 2024
Accepted: 09 December 2024
Published: 12 December 2024

http://www.aimspress.com/journal/Materials

Research article

Atomistic investigation of effect of twin boundary on machinability in diamond cutting of nanocrystalline 3C-SiC

Liang Zhao[1], Weimian Guan[1], Jiwen Xu[1], Zhiyuan Sun[1], Maoda Zhang[1] and Junjie Zhang[2,*]

[1] Shenyang Aircraft Industry (Group) Co., Ltd., Shenyang 110850, China
[2] Center for Precision Engineering, Harbin Institute of Technology, Harbin 150001, China

* **Correspondence:** Email: zhjj505@gmail.com.

Abstract: The machinability of hard brittle nanocrystalline cubic silicon carbide (3C-SiC) is strongly dependent on internal microstructure and its adapted machining response. Here, we conducted molecular dynamic simulations to explore the machinability of nanotwinned 3C-SiC with a large number of twin boundaries in diamond cutting. The effect of the introduction of twin boundaries on the diamond cutting of nanocrystalline 3C-SiC, particular for its contribution to suppressing brittle fracture and improving ductile-mode cutting, was investigated in-depth. Our simulation results revealed that twin boundaries exerted a significant impact on the deformation mechanism and subsequent surface integrity of nanocrystalline 3C-SiC. Specifically, intergranular fracture was significantly suppressed by the introduction of twin boundaries. In addition, various deformation behaviors such as phase transformation, crack propagation, dislocation activity, and twin boundary-associated deformation mechanisms were operated in cutting process of nanotwinned 3C-SiC. Furthermore, the influence of twin boundary spacing on the diamond cutting characteristics of nanotwinned 3C-SiC was also addressed.

Keywords: nanocrystalline 3C-SiC; ductile machinability; twin boundary; diamond cutting; molecular dynamics simulation

1. Introduction

Hard brittle nanocrystalline cubic silicon carbide (3C-SiC) is frequently employed in nanoelectromechanical systems (NEMS) due to its exceptional physical, thermal, and mechanical

characteristics [1–3]. Surface integrity plays an important role in the photoelectric conversion performance of 3C-SiC-based NEMS devices [4,5]. The ultra-precision single point diamond cutting is an eminent technology for the preparation of ultra-smooth surface due to its nanoscale machining accuracy [6–9]. To obtain high surface integrity of hard brittle materials by diamond cutting, it is critical to achieve ductile-mode cutting by diamond cutting [10–13]. However, achieving ultra-smooth surface of hard brittle nanocrystalline 3C-SiC within ductile regime by diamond cutting presents a challenge due to its intrinsic brittleness and high hardness compounded by robust covalent bonds [14,15].

The material removal mechanism of nanocrystalline 3C-SiC in diamond cutting has been revealed through atomic scale molecular dynamics (MD) simulations. Mishra et al. conducted MD simulations to elucidate the atomistic mechanisms underlying the ductility-controlled wear and friction in nanocrystalline 3C-SiC [16]. Liu et al. demonstrated the realization of ductile-mode cutting of nanocrystalline 3C-SiC through amorphization by performing MD simulations [17,18]. However, the mentioned researchers mainly focus on the ductile material removal of nanocrystalline 3C-SiC in diamond cutting, and there is a lack of in-depth understanding of its brittle failure mechanism in diamond cutting. Moreover, Zhao et al. concluded that the brittle failure of nanocrystalline 3C-SiC in diamond cutting is dominated by the initiation and propagation of cracks along grain boundaries (intergranular fracture) [19–21]. Therefore, suppressing intergranular fracture through ductile-mode cutting is vital for attaining ultra-high surface quality of nanocrystalline 3C-SiC.

In recent years, the emergence of nanotwinned materials containing a large number of twin boundaries (TBs) has provided an idea for the preparation of ultra smooth surfaces of nanocrystalline 3C-SiC. Specifically, compared with twin-free materials, nanotwinned materials have higher strength due to the obstruction of dislocation movement by TBs, as well as enhanced ductile deformation ability due to the presence of more dislocation nucleation sites provided by twin boundaries, which may facilitate the ductile-mode cutting of nanocrystalline 3C-SiC accompanied by suppressed intergranular fracture. However, research on nanotwinned 3C-SiC materials under different types of loading is limited. Chavoshi et al. explored the deformation mechanisms in nanotwinned 3C-SiC under compression and tension loading using MD simulations [22]. They also studied the compression-tension asymmetry in ductility of nanotwinned 3C-SiC [23]. Wang et al. performed MD simulations to report the compressive and tensile mechanical deformation of nanotwinned 3C-SiC nanowires [24]. Lin et al. reported the compressibility of periodically nanotwinned 3C-SiC nanowires using in situ high pressure X-ray diffraction [25].

While studies have offered valuable insights into the deformation mechanisms of nanotwinned 3C-SiC, a comprehensive understanding of diamond cutting on nanotwinned 3C-SiC through MD simulation remains incomplete. Specifically, the effect of the introduction of twin boundaries on the diamond cutting of nanocrystalline 3C-SiC is unknown, particularly for its contribution to suppressing brittle fracture and improving ductile-mode cutting. In diamond cutting of nanotwinned 3C-SiC, various deformation behaviors like phase transformation, crack propagation, dislocation activity and twin boundary-associated mechanisms are at play. However, the specific contributions of each mode to the overall cutting process remain unclear. Moreover, the properties of the workpiece material significantly impact the ultra-precision cutting process. This adds complexity to understanding the diamond cutting mechanisms of nanotwinned 3C-SiC due to its intricate deformation behavior. Therefore, there is a compelling need to understand the effect of twin boundary on the cutting characteristics of nanocrystalline 3C-SiC.

In this research, we conduct MD simulations to explore the machinability of nanotwinned 3C-SiC in diamond cutting. We examine how twin boundaries affect cutting mechanisms by analyzing changes in cutting force, defect formation and intergranular fracture. Through our investigations, we reveal that twin boundaries exert a significant impact on the deformation mechanism and subsequent surface integrity of nanocrystalline 3C-SiC. Specifically, intergranular fracture is significantly suppressed by the introduction of twin boundaries. Furthermore, the influence of twin boundary spacing (TBS) on diamond cutting characteristics of nanotwinned 3C-SiC is addressed.

2. Materials and methods

The lattice structure of 3C-SiC consists of two intersecting face-centered cubic (FCC) lattices. Accordingly, coherent twin boundary in nanotwinned 3C-SiC lies on the {111} plane, which is similar to FCC metal. Asymmetric silicon-carbon bonding twins have been proven to be the most stable twin structure in 3C-SiC [26]. Figure 1 displays the MD model employed in this study for diamond cutting of nanotwinned 3C-SiC, which comprises a nanotwinned 3C-SiC workpiece and a rigid tool. The detailed parameters utilized in current MD simulations are summarized in Table 1. Periodic boundary conditions are exclusively implemented in the Z direction of the workpiece. Vashishta and Morse potentials are utilized to describe bonding and non-bonding interactions in diamond cutting process of 3C-SiC, respectively [27–29].

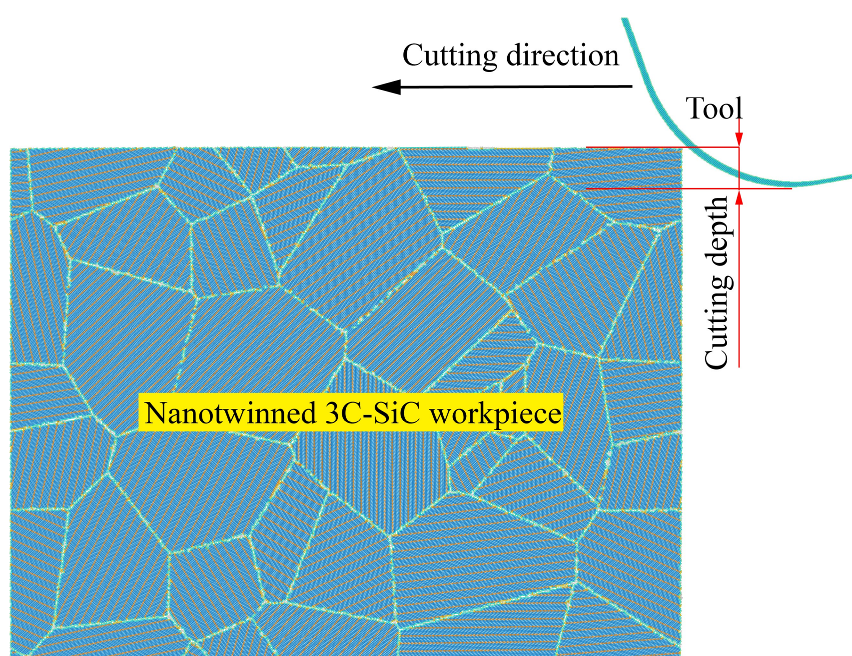

Figure 1. MD model of orthogonal cutting of nanotwinned 3C-SiC.

The {111} twin boundary of nanotwinned 3C-SiC is created by following the same modeling strategy as in the study by Chavoshi et al. [23]. We consider twin-free and five different twin boundary spacings: 1.5 (TBS1), 3 (TBS2), 6 (TBS3), 9 (TBS4), and 12 nm (TBS5), to examine their impact on the cutting process. In the present work, atoms are color-coded by identification algorithm of diamond structure according to the following scheme [30]: blue represents pristine diamond lattice atoms, gray denotes amorphous atoms, orange indicates twin boundary atoms, and green signifies

grain boundary atoms. MD simulations are executed through LAMMPS package with a timestep of 1 fs [31].

Table 1. Utilized parameters in MD simulations of nanotwinned 3C-SiC diamond cutting.

Parameters	Value
Workpiece dimension	130 × 100 × 2 nm
Number of grains	32
Edge radius of tool	30 nm
Rake angle of tool	–20°
Clearance angle of tool	10°
Cutting speed	400 m/s
Cutting depth	8 nm

3. Results and discussion

3.1. Nanotwinned 3C-SiC versus twin-free 3C-SiC

Initial MD simulations of orthogonal cutting focus on exploring the machining characteristics of nanotwinned 3C-SiC with TBS of 6 nm and twin-free 3C-SiC using identical machining parameters. Three force components are observed on the diamond cutting tool: Cutting force, thrust force, and lateral force. Figure 2a,b illustrate changes in cutting force and thrust force over the cutting length during the machining process for twin-free and nanotwinned 3C-SiC substrate, respectively. Figure 2a highlights distinct cutting force characteristics in various cutting regimes for both nanotwinned and twin-free 3C-SiC. The cutting process for twin-free 3C-SiC can be segmented into the following five regimes: regime I—elastic deformation and plastic deformation governed by dislocation activity; regime II—brittle failure dominated by intergranular fracture; regime III—plastic deformation dominated by deformation twinning; regime IV—brittle failure dominated by intergranular fracture; and regime V—brittle mode dominated deformation under the competition of crack propagation and coalescence. For nanotwinned 3C-SiC, the cutting process can be segmented into the following three regimes: regimes I and II exhibit similar force characteristics as twin-free 3C-SiC, regime III—plastic deformation dominated by twin boundary-associated deformation.

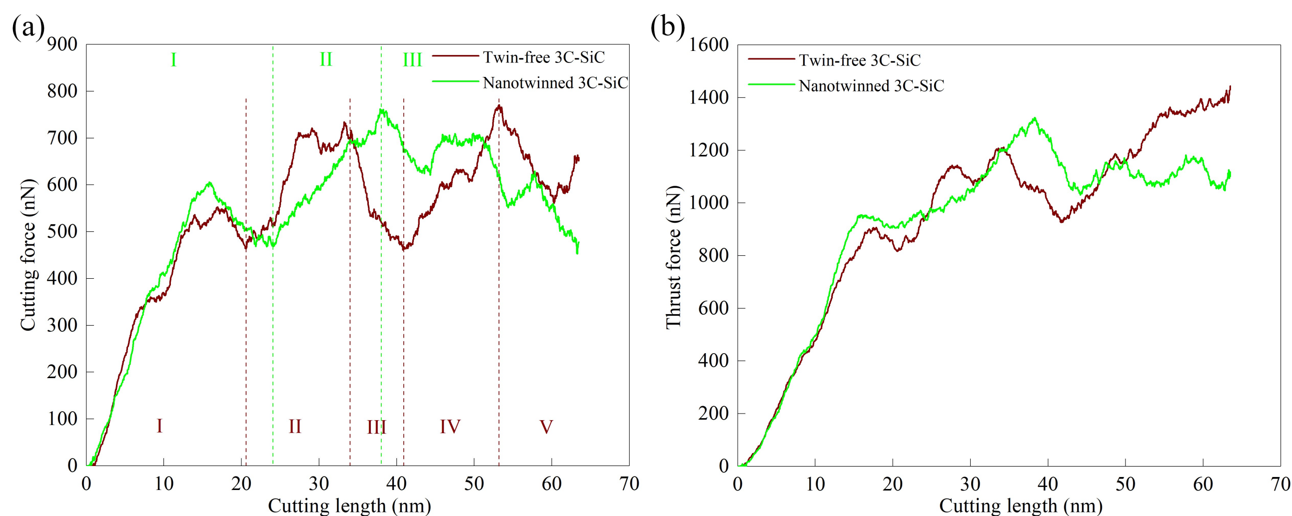

Figure 2. Changes in machining force during diamond cutting of both nanotwinned 3C-SiC and twin-free 3C-SiC. (a) Cutting force; (b) thrust force.

As the cutting tool engages the right side of the 3C-SiC substrate, the material initially undergoes elastic deformation, leading to a sharp rise in cutting force. In the late stage of regime I, the cutting force undergoes a rapid decline due to material yielding accompanied with dislocation nucleation from the free surface. The plastic deformation dominated by strong dislocation activity leads to a decrease in cutting force, i.e., ductile-mode cutting. In regime II the cutting force increases rapidly due to the occurrence of severe intergranular fracture events caused by crack initiation and propagation at the grain boundary junctions, i.e., brittle-mode cutting. Intergranular fracture within the 3C-SiC substrate arises from the buildup of internal strain energy along grain boundaries, resulting in the breaking of bonds between neighboring atoms within these boundaries. However, the rise slope of cutting force of twin-free 3C-SiC is larger than that in nanotwinned 3C-SiC. The dynamic analysis of defect evolution shows that there is only one main crack initiating and propagating at the grain boundary junction in nanotwinned 3C-SiC, while there are two major cracks propagating simultaneously in twin-free 3C-SiC, which results in a larger rise slope of cutting force compared to nanotwinned SiC, as shown in Figure 3. Figure 3a,b show the machining morphology of twin-free and nanotwinned 3C-SiC around cutting tool at the cutting length of 32 nm in regime II, respectively. As shown in Figure 3, although there is similar machined surface quality for all twin-free and nanotwinned 3C-SiC substrate, the crack propagation events inside the substrate differ significantly between them. Figure 3 demonstrates that there are more intergranular crack nucleation sites in twin-free 3C-SiC due to the absence of accommodation of plastic strain mediated by the twin boundaries.

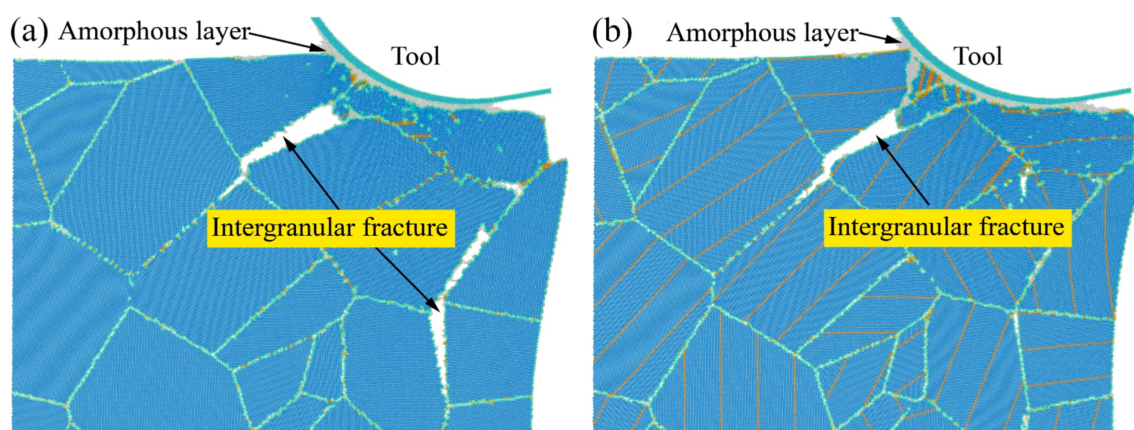

Figure 3. MD results of machined morphology of twin-free and nanotwinned 3C-SiC in orthogonal cutting at cutting length of 32 nm. (a) Twin-free 3C-SiC and (b) nanotwinned 3C-SiC.

Upon advancement of the cutting tool, two twin boundaries, namely TB1 and TB2, form within a grain by the splitting of the intrinsic stacking fault originating from the grain boundary triple junction, as shown in Figure 4a. Deformation twinning tends to be emitted from a grain boundary and then terminates near another grain boundary. This process is accompanied by a significant reduction in cutting force during regime III for twin-free 3C-SiC. Accordingly, the dynamic analysis of atomic evolution reveals a notable increase in twin boundary atoms during the later stage of regime III. Upon nucleation, the twin plane shifts by an atomic step through twin boundary migration to attain stability, as depicted in Figure 4b. In addition, the degree of intergranular fracture increases slightly compared to regime II. This suggests that the cutting force evolution is influenced by intense competition between intergranular fracture (crack initiation and propagation along grain boundary) and deformation twinning. Specifically, deformation twinning in the grain significantly influences the mechanical deformation of twin-free 3C-SiC in regime III. For twin-free 3C-SiC, the cutting force rises again rapidly in regime IV, indicating the onset of more severe intergranular fracture events. The dynamic analysis of defect evolution shows that there are more cracks initiation and propagation along the grain boundary junctions. The simultaneous propagation of multiple major cracks results in a rapid increase for cutting force, i.e., intergranular fracture dominated brittle-mode cutting. In addition, the TB1 and TB2 formed in regime III remain stable during the cutting process. It is worth noting that no new intergranular fracture is formed in the nanotwinned 3C-SiC in this cutting regime, and the previously formed main crack did not further propagate along the grain boundary junction due to the accommodation of strain energy provided by the twin boundaries. This suggests that the introduction of twin boundaries can suppress intergranular fracture and improve ductile-mode cutting of nanocrystalline 3C-SiC.

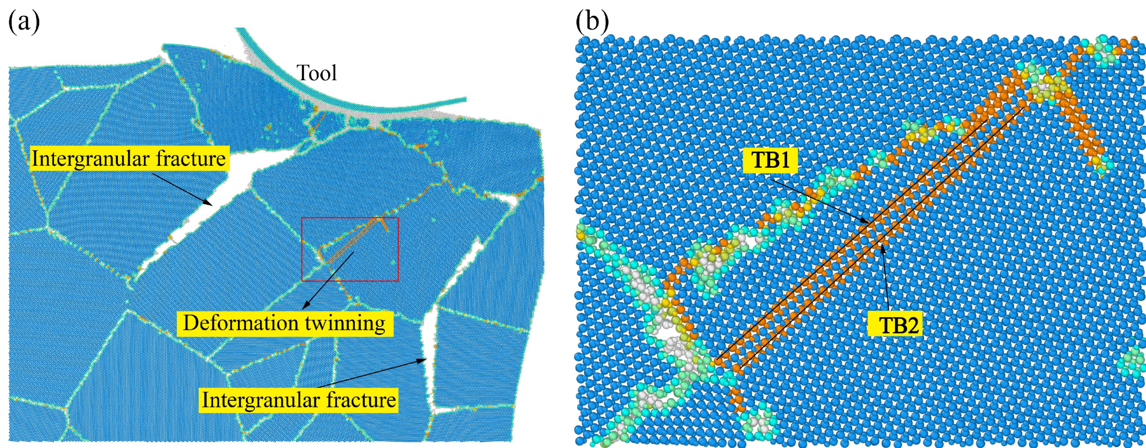

Figure 4. (a) Deformation twinning formed during cutting process on twin-free 3C-SiC. (b) Close-up of TB1 and TB2.

Although both cutting force of regime V for twin-free 3C-SiC and regime III for nanotwinned 3C-SiC show a significant downward trend, the underlying deformation mechanisms between them are different. To further understand the difference in the deformation mechanism between them, dislocation evolution during diamond cutting is assessed through dislocation extraction algorithm (DXA) analysis of the defect zone surrounding the cutting tool. Figure 5a,b depict the activating dislocations at a cutting length of 60 nm for twin-free and nanotwinned 3C-SiC, respectively. Dislocations are visualized as thin tubes, with blue representing 1/2[110] perfect dislocations and green representing 1/6[112] Shockley partial dislocations. The dislocation density in nanotwinned 3C-SiC is much larger than that in twin-free 3C-SiC around cutting tool, which will improve the machinability by ductile-mode cutting due to the softening prompted by dislocation emission from twin boundaries as well as dislocation glide along twin boundaries. Figure 5 also demonstrates that the number and distribution area of dislocations in nanotwinned 3C-SiC are larger than that in twin-free 3C-SiC. In addition, the material accumulation in front of the cutting tool is more pronounced due to the annihilation of dislocations on the free surface.

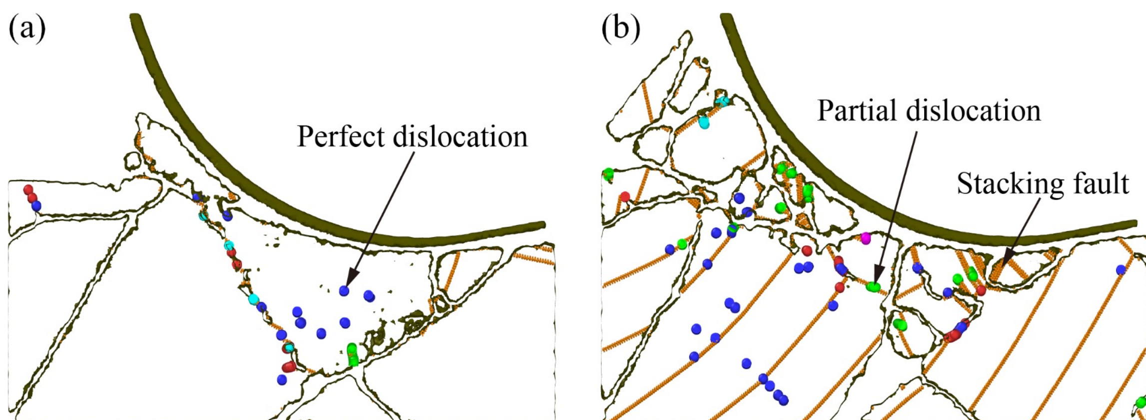

Figure 5. Activating dislocations distribution for twin-free and nanotwinned 3C-SiC at a cutting length of 60 nm. (a) Twin-free 3C-SiC and (b) nanotwinned 3C-SiC.

Compared with nanotwinned 3C-SiC, twin-free 3C-SiC exhibits a significantly different deformation mechanism in regime V. Specifically, one of the intergranular main cracks formed in previous regime disappears accompanied by the coalescence of adjacent grains, which leads to a rapid decrease of cutting force in the former period of regime V. However, the cutting force increased rapidly in the later period of regime V due to the increased crack initiation and propagation along the grain boundaries, i.e., severe intergranular fracture events. Figure 6 shows the structure configuration of twin-free and nanotwinned 3C-SiC substrates after diamond cutting, highlighting the significant impact of twin boundary on the deformation mechanism of 3C-SiC. Figure 6 also clearly demonstrates that the intergranular fracture is the primary failure mechanism for nanocrystalline 3C-SiC. Compared to twin-free 3C-SiC, intergranular fracture is significantly suppressed in nanotwinned 3C-SiC, which can be attributed to accommodation of compatibility stresses provided by twin boundaries. It should be noted that crack initiation and propagation along grain boundaries (intergranular fracture) inside the workpiece have important influences on performance of 3C-SiC-based devices. This will seriously degrade the performance of 3C-SiC-devices and should be avoided as much as possible. In addition, numerous partial dislocations glide parallel to the twin plane and annihilate on the free surface of nanotwinned 3C-SiC, which causes more pronounced material accumulation in front of the cutting tool. For both twin-free and nanotwinned 3C-SiC, the amorphization occurs in the contact area between the workpiece and cutting tool due to high stress levels, leading to rapid lattice destruction.

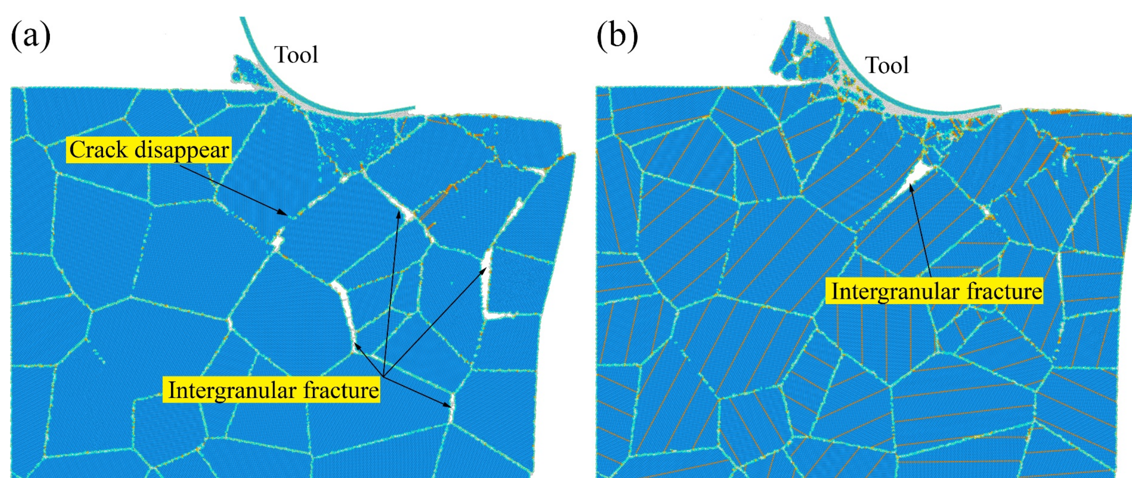

Figure 6. MD snapshots of cutting configurations at a cutting length of 64 nm. (a) Twin-free 3C-SiC and (b) nanotwinned 3C-SiC.

Figure 7 shows the intergranular fracture inside twin-free 3C-SiC substrate during the cutting process at an atomic scale level. As the advancement of cutting tool and with the increase of strain, the initial nucleation of the cavity along grain boundaries occurs at the critical strain. The material between adjacent cavities can be considered stretch sample with neck shrinkage. The neck is pulled out at atomic scale to form a single atomic chain in alternating arrangements of carbon and silicon atoms before it finally breaks. It should be noted that these chains will maintain a metastable state in a separate equilibrium simulation system in which the strain is remained and the stress can be relaxed. For twin-free 3C-SiC, stress relaxation can be achieved by the plastic flow along grain boundaries. Although the disordered intergranular membrane in nanocrystal 3C-SiC exhibits ductility, its plastic

deformation is constrained by neighboring grains. Consequently, large multi-axial stresses will be applied to grain boundaries during mechanical loading, which can promote cavity nucleation. The final intergranular fracture will occur until the cavities percolate through the intergranular membrane. It is important to note that no new lattice instability or dislocation nucleation is observed in the grains near the fractured intergranular film. This suggests that intergranular fracture is primarily driven by cavity nucleation and their propagation within a confined intergranular film. However, for nanotwinned 3C-SiC, intergranular fracture can be significantly suppressed by the introduction of twin boundaries.

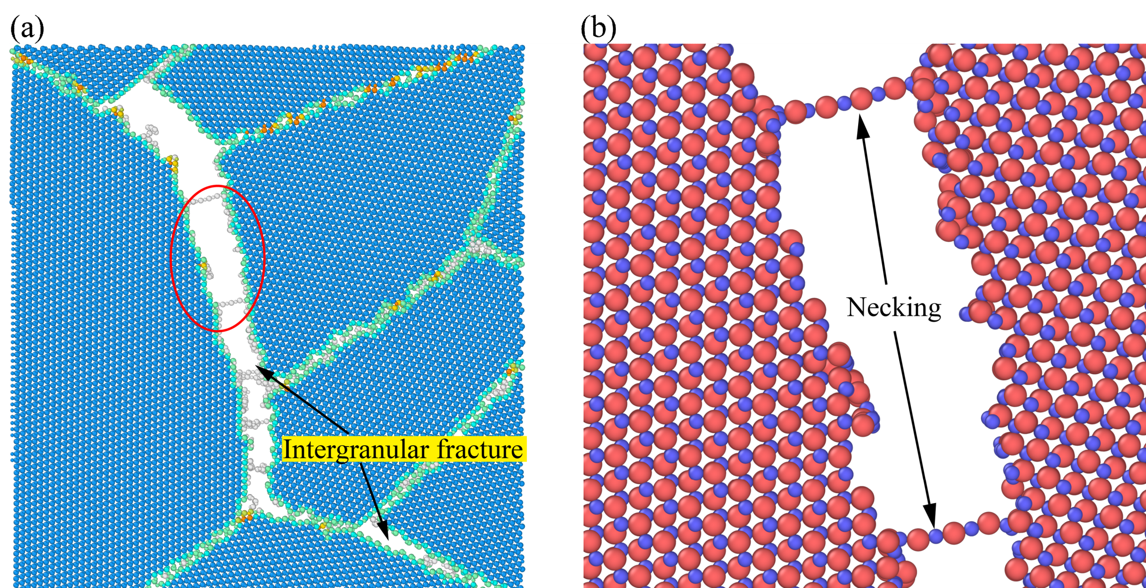

Figure 7. (a) Intergranular fracture inside twin-free 3C-SiC; (b) close-up of necking to form single-layered chains of alternating arrangements of Si (red) and C (blue) atoms.

3.2. Influence of twin boundary spacing

Figure 8a,b depict changes in cutting force and thrust force with cutting length for different TBS. The friction coefficient, defined as the ratio of cutting force to thrust force, is shown in Figure 8c. These curves exhibit similar trends: frictional resistance rises rapidly during cutting and stabilizes around a constant average value as cutting progresses. Figure 8d displays the constant average friction coefficient values between cutting lengths of 30 and 64 nm for nanotwinned and twin-free 3C-SiC substrate, with error bars indicating the range of values for each substrate. Fluctuations in friction coefficient towards the end of cutting are attributed to the heterogeneous nature of brittle fracture and plastic deformation, with the constant average value strongly influenced by TBS. Specifically, it initially decreases with decreasing TBS, reaching a minimum for TBS2 with a spacing of 3 nm, and then increases with further decreases in TBS. This suggests the presence of a critical TBS of 3 nm where the constant average friction coefficient value is minimized.

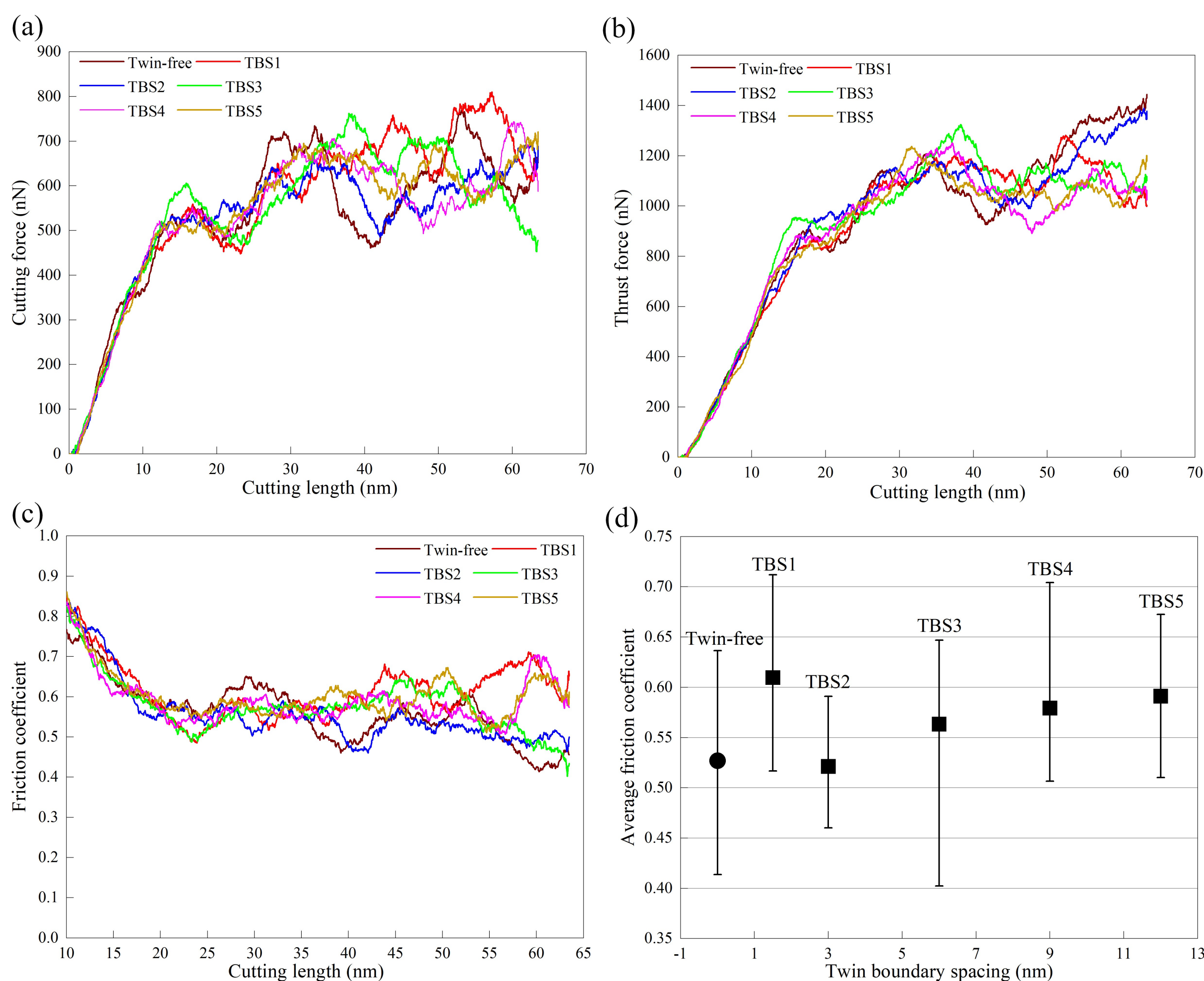

Figure 8. Diamond cutting of nanotwinned 3C-SiC with varying TBS. (a) Cutting force; (b) thrust force; (c) friction coefficient–cutting length curves; and (d) average friction coefficient.

Figure 9a,b display changes in normalized quantities of twin boundary atoms and amorphous atoms after diamond cutting on nanotwinned 3C-SiC substrates, respectively. The normalized number denotes the proportion of the change in count relative to the initial count of various atom types. It is evident that when TBS equals or exceeds the critical value (TBS2), the TB atom count increases alongside an uptick in amorphous atoms during diamond cutting. Furthermore, this increase in TB atoms is more pronounced for larger TBS. Conversely, the TB atom count decreases after diamond cutting on TBS1, where the TBS is less than the critical value (TBS2). This highlights the critical TBS for achieving the minimum constant average friction coefficient value, influenced by the fierce competition among deformation twinning, intergranular fracture and twinning migration. In addition, for both nanotwinned 3C-SiC substrates, the number of amorphous atoms significantly increase after diamond cutting.

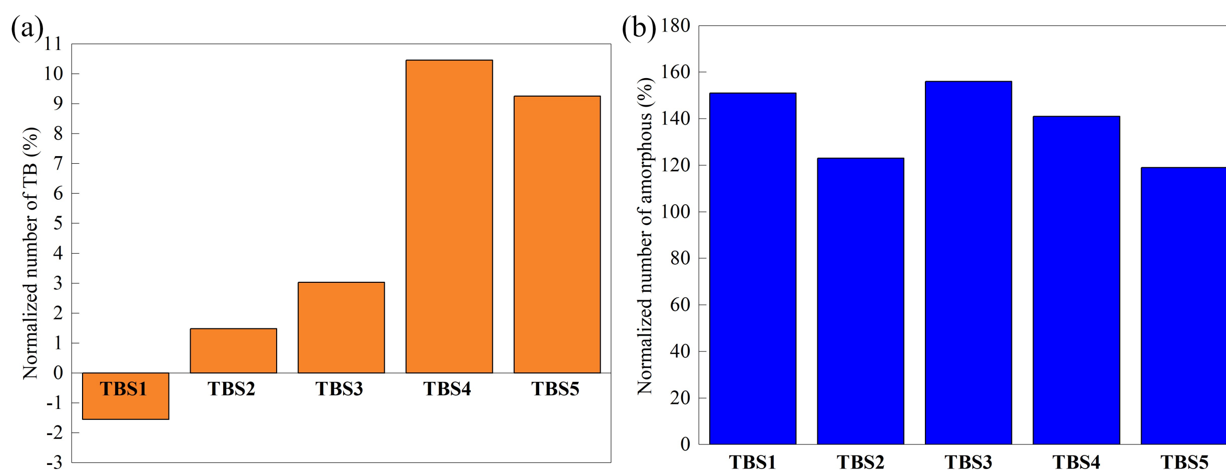

Figure 9. Changes in normalized numbers of (a) twin boundary atoms and (b) amorphous atoms after diamond cutting for nanotwinned 3C-SiC with different TBS.

Figure 10 illustrates the machined surface morphologies of different nanotwinned 3C-SiC substrates after diamond cutting. For TBS1 with a high density of twin boundaries, the twin boundaries inside the grain directly below the tool are destroyed to a greater extent as the tool passes through the workpiece, where the stress is large enough to destroy the coherent twin structure, as shown in Figure 10a. Compared with twin-free 3C-SiC, intergranular fracture is significantly suppressed for all nanotwinned 3C-SiC substrates, which can be attributed to the accommodation of compatibility stresses provided by twin boundaries. Therefore, the introduction of twin plan structure enhances the ductility and decrease brittle fracture of nanocrystalline 3C-SiC. Specifically, there is no main crack of intergranular fracture on TBS1 after diamond cutting, and the most severe brittle fracture occur on TBS2 among nanotwinned 3C-SiC substrates. This clearly highlights the strong dependence of intergranular fracture on the TBS. Figure 10 highlights the significant impact of TBS on the surface pileup distribution in nanotwinned 3C-SiC substrates, owing to variations in the glide directions of slip systems. Notably, the twin-free 3C-SiC substrate exhibits a smaller surface pileup volume compared to its nanotwinned 3C-SiC counterparts. In nanotwinned 3C-SiC substrates, surface pileup becomes more pronounced with larger TBS values, particularly when TBS equals or exceeds the critical threshold (TBS2). Surface pileup arises from the buildup of surface steps generated when dislocation motion, gliding on <110>{111} slip systems, ceases at the surface. Despite a higher dislocation density in nanotwinned 3C-SiC substrates with smaller TBS, fewer active slip systems exist as dislocations predominantly glide parallel to twin boundaries. Conversely, in nanotwinned substrates with larger TBS values, there is more space available for dislocation multiplication.

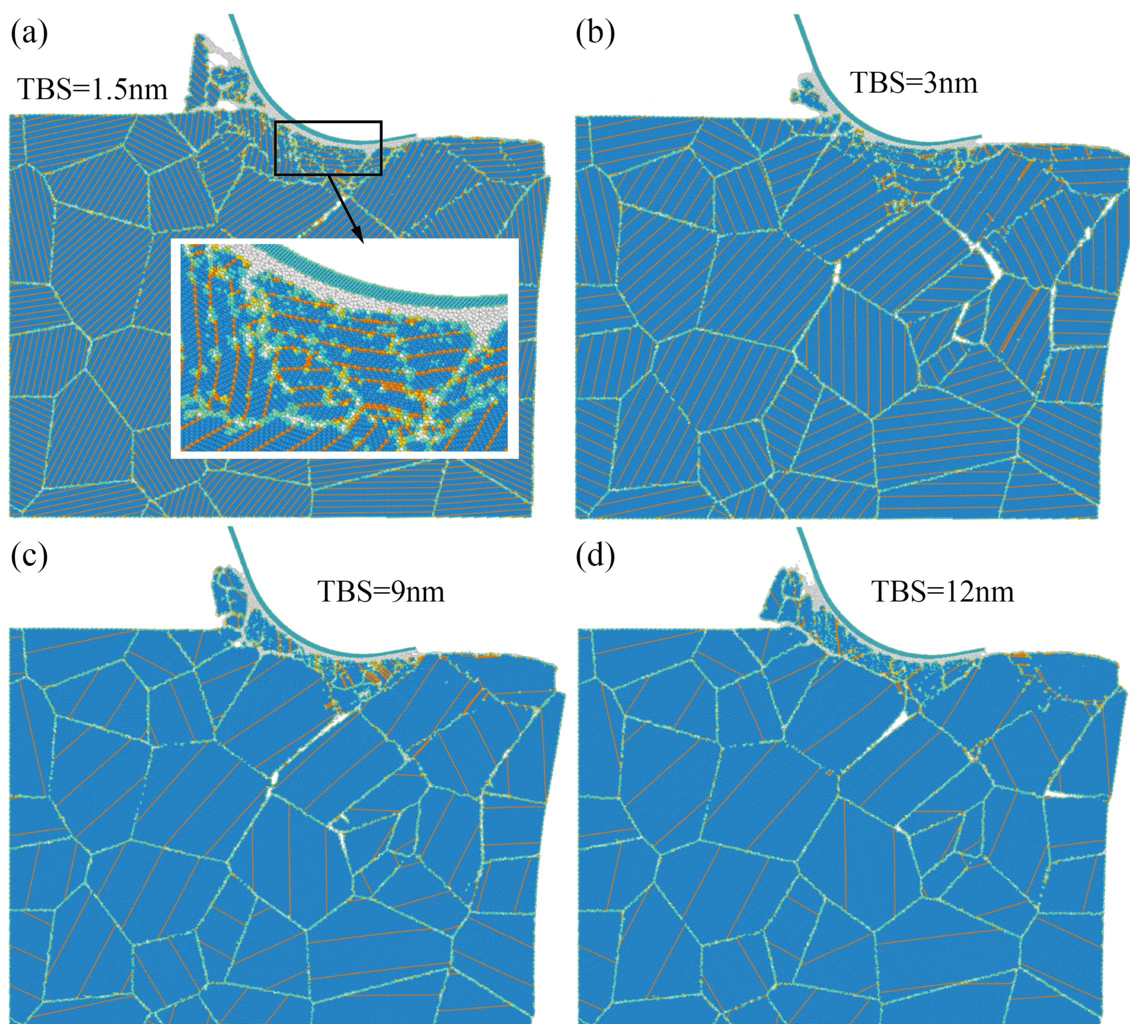

Figure 10. Resulting machined surface morphologies of various nanotwinned 3C-SiC substrates after diamond cutting. (a) TBS1; (b) TBS2; (c) TBS4; and (d) TBS5.

In addition, twin boundary migration tends to occur for nanotwinned 3C-SiC with smaller TBS. Figure 11 offers a detailed glimpse into the atomic layout of the coherent twin boundary during twin boundary migration for TBS2. Under increasing mechanical loading, resulting in higher resolved shear stress on the twin plane, the twin boundary shifts direction perpendicular to itself by two atomic planes. This movement is facilitated by twinning partial dislocation at the coherent twin boundary accompanied by a step (Figure 11b). Twinning dislocations propagating and gliding along the twin plane result in step formation, which may ultimately initiate twin boundary migration by two atomic layers. Consequently, shear-induced dislocation motion along the coherent twin boundary generates twin boundary steps and triggers twin plane migration, disrupting the coherency of the twin boundary and creating local stress concentration sites along them. Additionally, as depicted in Figure 11b, the lattice dislocation originating from the defective coherent twin boundary at the step location develop by generating intrinsic stacking faults (ISF), which are dragged behind. It should be noted that in addition to the influence of twin-related dislocation behavior on the machinability of nanocrystalline 3C-SiC, the characteristics of the grain boundaries, such as stability and strength, also significantly impact the generation and propagation of cracks. For instance, the

macroscopic degrees of freedom of a flat grain boundary between two grains with a definite orientation relationship are specific. In the presence of twins, the grain boundary will contain multiple segments with different macroscopic degrees of freedom, and the properties of the grain boundary will differ significantly from that in the absence of twins. The changes in the grain boundary structure and topological properties of the grain boundary networks caused by the introduction of twins, and their role in the fracture behavior cannot be ignored. Furthermore, the triple points where the TBs intersect with grain boundaries are the main stress concentration regions, which is also the main reason why twinning partials are easily activated and lead to TB migration or detwinning process.

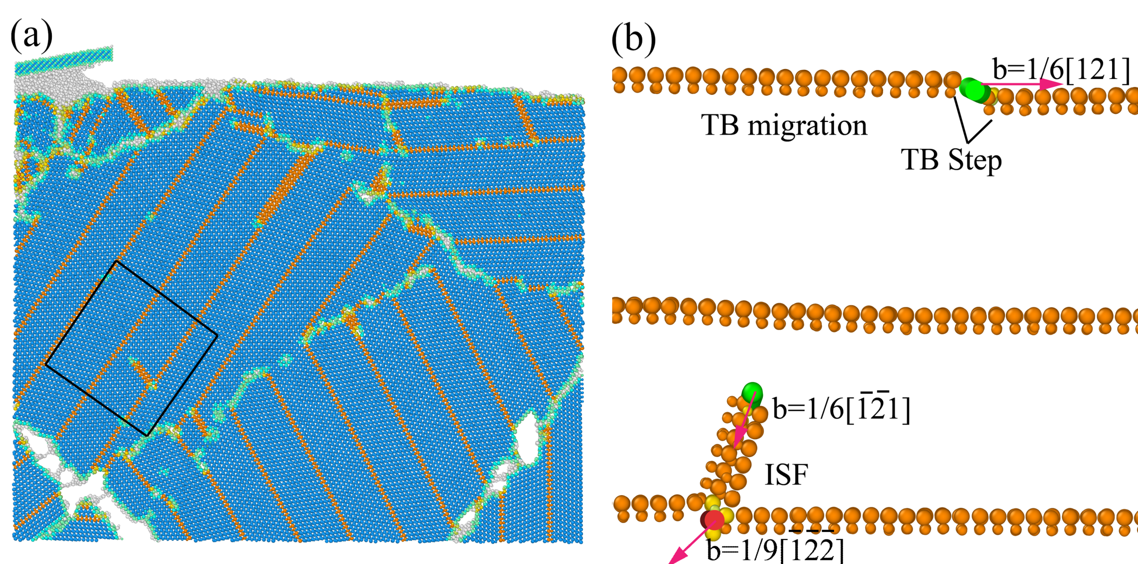

Figure 11. (a) Lots of twin planes migrate on nanotwinned 3C-SiC substrate with TBS2; and (b) enlarged view of coherent twin boundary illustrating the formation of step and nucleation of partial dislocation.

4. Conclusions

In conclusion, we perform MD simulations to study the diamond cutting mechanisms of nanotwinned 3C-SiC with an emphasis on improving its ductile cutting performance. The effect of twin boundary on cutting mechanisms of nanocrystalline 3C-SiC is systematically investigated by analyzing changes in cutting force, dislocation activity, intergranular fracture, and twin boundary-mediated deformation behavior. The simulation results demonstrate that there are more nucleation sites of intergranular crack for twin-free 3C-SiC workpiece due to the absence of accommodation of plastic strain mediated by the twin boundaries. The dislocation density in nanotwinned 3C-SiC is much larger than that in twin-free 3C-SiC, which will improve the machinability due to the softening prompted by dislocation emission from twin boundaries as well as dislocation glide along twin boundaries. In addition, intergranular fracture is primarily driven by cavity nucleation and their propagation within a confined intergranular film. In particular, intergranular fracture can be significantly suppressed by the introduction of twin boundaries in diamond cutting of nanocrystalline 3C-SiC. Additionally, the ductile machinability of

nanotwinned 3C-SiC is strongly dependent on the twin boundary spacing. Specifically, for twin boundary spacing from 1.5 (TBS1) to 12 nm (TBS5), there exists a critical TBS of 3 nm (TBS2) where the surface pile-up and constant average friction coefficient value are minimized. There is no main crack of intergranular fracture on TBS1 after diamond cutting, and the most severe brittle fracture occurs on TBS2 among all nanotwinned 3C-SiC substrates.

Use of AI tools declaration

The authors declare they have not used Artificial Intelligence (AI) tools in the creation of this article.

Acknowledgement

The authors gratefully acknowledge the National Natural Science Foundation of China (No. 52275416).

Author contributions

Liang Zhao and Junjie Zhang are involved in conceptualization, methodology and calculations, writing original draft, resources, funding acquisition. Weimian Guan and Jiwen Xu are involved in review and editing and discussion. Zhiyuan Sun and Maoda Zhang are involved in methodology and validation. All authors have read and agreed to the published version of the manuscript.

Conflict of interest

Junjie Zhang is an editorial board member for *AIMS Materials Science* and was not involved in the editorial review or the decision to publish this article. The authors declare no conflict of interest.

Reference

1. Huang XMH, Zorman CA, Mehregany M, et al. (2023) Nanodevice motion at microwave frequencies. *Nature* 421: 496–497. https://doi.org/10.1038/421496a
2. Yang X, Yang XZ, Sun RY, et al. (2019) Obtaining atomically smooth 4H-SiC (0001) surface by controlling balance between anodizing and polishing in electrochemical mechanical polishing. *Nanomanuf Metrol* 2: 140–147. https://doi.org/10.1007/s41871-019-00043-5
3. Mehregany M, Zorman CA, Rajan N, et al. (1998) Silicon carbide MEMS for harsh environments. *P IEEE* 86: 1594–1609. https://doi.org/10.1109/5.704265
4. Ekinci KL (2005) Electromechanical transducers at the nanoscale: actuation and sensing of motion in nanoelectromechanical systems (NEMS). *Small* 1: 786–97. https://doi.org/10.1002/smll.200500077
5. Yoon HS, Park B, Jun SC (2013) Surface roughness effects on the frequency tuning performance of a nanoelectromechanical resonator. *Nanoscale Res Lett* 8: 270. https://doi.org/10.1186/1556-276X-8-270

6. Lee YJ, Wang H (2021) Characterizing crack morphology toward improving ductile material removal of calcium fluoride. *Ceram Int* 47: 28543–28556. https://doi.org/10.1016/j.ceramint.2021.07.012
7. Luo XC, Goel S, Reuben RL (2012) A quantitative assessment of nanometric machinability of major polytypes of single crystal silicon carbide. *J Eur Ceram Soc* 32: 3423–3434. https://doi.org/10.1016/j.jeurceramsoc.2012.04.016
8. Wu ZH, Liu WD, Zhang LC (2017) Revealing the deformation mechanisms of 6H-silicon carbide under nano-cutting. *Comp Mater Sci* 137: 282–288. https://doi.org/10.1016/j.commatsci.2017.05.048
9. Tian Z, Chen X, Xu X (2020) Molecular dynamics simulation of the material removal in the scratching of 4H-SiC and 6H-SiC substrates. *Int J Extreme Manuf* 2: 045104. https://doi.org/10.1088/2631-7990/abc26c
10. Chavoshi SZ, Luo XC (2016) Molecular dynamics simulation study of deformation mechanisms in 3C-SiC during nanometric cutting at elevated temperatures. *Mat Sci Eng A-Struct* 654: 400–417. https://doi.org/10.1016/j.msea.2015.11.100
11. Wu Z, Liu W, Zhang L, et al. (2020) Amorphization and dislocation evolution mechanisms of single crystalline 6H-SiC. *Acta Mater* 182: 60–67. https://doi.org/10.1016/j.actamat.2019.10.037
12. Goel S, Stukowski A, Luo XC, et al. (2013) Anisotropy of single-crystal 3C-SiC during nanometric cutting. *Modell Simul Mater Sci Eng* 21: 065004. https://doi.org/10.1088/0965-0393/21/6/065004
13. Xiao GB, To S, Zhang GQ (2015) The mechanism of ductile deformation in ductile regime machining of 6H SiC. *Comp Mater Sci* 98: 178–188. https://doi.org/10.1016/j.commatsci.2014.10.045
14. Tian D, Xu Z, Liu L, et al. (2021) In situ investigation of nanometric cutting of 3C-SiC using scanning electron microscope. *Int J Adv Manuf Tech* 115: 2299–2312. https://doi.org/10.1007/s00170-021-07278-x
15. Zhang T, Jiang F, Huang H, et al. (2021) Towards understanding the brittle–ductile transition in the extreme manufacturing. *Int J Extreme Manuf* 3: 022001. https://doi.org/10.1088/2631-7990/abdfd7
16. Mishra M, Tangpatjaroen C, Szlufarska I (2014) Plasticity-controlled friction and wear in nanocrystalline SiC. *J Am Ceram Soc* 97: 1194–1201. https://doi.org/10.1111/jace.12810
17. Liu Y, Li B, Kong L (2018) Molecular dynamics simulation of silicon carbide nanoscale material removal behavior. *Ceram Int* 44: 11910–11913. https://doi.org/10.1016/j.ceramint.2018.03.195
18. Liu Y, Li B, Kong L (2018) A molecular dynamics investigation into nanoscale scratching mechanism of polycrystalline silicon carbide. *Comp Mater Sci* 148: 76–86. https://doi.org/10.1016/j.commatsci.2018.02.038
19. Zhao L. Hu WJ, Zhang Q, et al. (2021) Atomistic origin of brittle-to-ductile transition behavior of polycrystalline 3C-SiC in diamond cutting. *Ceram Int* 47: 23895–23904. https://doi.org/10.1016/j.ceramint.2021.05.098
20. Zhao L, Zhang JG, Fu YF, et al. (2022) Thermal softening-suppressed inter-granular embrittlement of polycrystalline 3C-SiC under diamond cutting. *Mater Design* 223: 111250. https://doi.org/10.1016/j.matdes.2022.111250

21. Zhao L, Zhang JJ, Zhang JG, et al. (2023) Numerical simulation of materials-oriented ultra-precision diamond cutting: review and outlook. *Int J Extreme Manuf* 5: 022001. https://doi.org/10.1088/2631-7990/acbb42
22. Chavoshi SZ, Tschopp MA, Branicio PS (2019) Transition of deformation mechanisms in nanotwinned single crystalline SiC. *Philos Mag* 99: 21. https://doi.org/10.1080/14786435.2019.1637033
23. Chavoshi SZ, Xu S (2018) Tension-compression asymmetry in plasticity of nanotwinned 3C-SiC nanocrystals. *J Appl Phys* 124: 095103. https://doi.org/10.1063/1.5046949
24. Wang ZG, Li JB, Gao F, et al. (2010) Tensile and compressive mechanical behavior of twinned silicon carbide nanowires. *Acta Mater* 58: 1963–1971. https://doi.org/10.1016/j.actamat.2009.11.039
25. Lin ZJ, Wang L, Zhang J, et al. (2010) Nanoscale twinning-induced elastic strengthening in silicon carbide nanowires. *Scripta Mater* 63: 981–984. https://doi.org/10.1016/j.scriptamat.2010.07.023
26. Chavoshi SZ, Xu S (2018) Twinning effects in the single/nanocrystalline cubic silicon carbide subjected to nanoindentation loading. *Materialia* 3: 304–325. https://doi.org/10.1016/j.mtla.2018.09.003
27. Vashishta P, Kalia RK, Nakano A, et al. (2007) Interaction potential for silicon carbide: A molecular dynamics study of elastic constants and vibrational density of states for crystalline and amorphous silicon carbide. *J Appl Phys* 101: 103515. https://doi.org/10.1063/1.2724570
28. Kikuchi H, Kalia RK, Nakano A, et al. (2005) Brittle dynamic fracture of crystalline cubic silicon carbide (3C-SiC) via molecular dynamics simulation. *J Appl Phys* 98: 103524. https://doi.org/10.1063/1.2135896
29. Zhao L, Zhang JJ, Zhang JG, et al. (2021) Atomistic investigation of machinability of monocrystalline 3C-SiC in elliptical vibration-assisted diamond cutting. *Ceram Int* 47: 2358–2366. https://doi.org/10.1016/j.ceramint.2020.09.078
30. Stukowski A, Bulatov VV, Arsenlis A (2012) Automated identification and indexing of dislocations in crystal interfaces. *Modelling Simul Mater Sci Eng* 20: 085007. https://doi.org/10.1088/0965-0393/20/8/085007
31. Plimpton S (1995) Fast parallel algorithms for short-range molecular dynamics. *J Comput Phys* 117: 1–19. https://doi.org/10.1006/jcph.1995.1039

AIMS Press

© 2024 the Author(s), licensee AIMS Press. This is an open access article distributed under the terms of the Creative Commons Attribution License (http://creativecommons.org/licenses/by/4.0)